Volume 20, No 3 | International Journal of Radiation Research, July 2022

Correlation in high resolution computed tomography signs with pathological subtype and differentiation degree of lung adenocarcinoma

L. Duan[#], W. Shan[#], L. Guo[*], G. Bo

Department of Medical Imaging, the Affiliated Huaian No.1 People's Hospital of Nanjing Medical University, Huai'an, 223300, China

► ***Original article***

***Corresponding author:**
Dr. Lili Guo,
***E-mail:** guolili163@163.com*

Received: August 2021
Final revised: February 2022
Accepted: March 2022

Int. J. Radiat. Res., July 2022; 20(3): 679-685

DOI: 10.52547/ijrr.20.3.23

[#] Contributed equally to this study.

Keywords: *Lung adenocarcinoma, computed tomography, sign, pathology, differentiation.*

ABSTRACT

***Background*:** To study the relationship between high-resolution computed tomography (HRCT) signs and the pathological subtypes and differentiation degree of lung adenocarcinoma. ***Materials and Methods*:** We retrospectively reviewed HRCT images of 394 lung adenocarcinoma cases and compared the diversity of images among preinvasive lesions (PILs), minimally invasive adenocarcinoma (MIA) and invasive adenocarcinoma (IAC) and the differentiation degrees of IAC by Kruskal-Wallis and χ^2 tests. ***Results*:** There were significant differences in the size, density and incidences of the pleura traction sign, spicule sign, lobulation sign, tumor vascular sign, bronchial cutoff sign, air bronchogram sign and cavity sign of PILs, MIA and IAC (χ^2=2.172~247.077, P<0.05). The incidences of all these signs (except for the cavity sign) in IAC were higher than those in the other two groups (P<0.05). There were no significant differences in margin irregularity or vacuole signs among PILs, MIA and IAC (P>0.05). There were significant differences in the size, density, and incidences of margin irregularity, the pleura traction sign, the spicule sign, the lobulation sign, the tumor vascular sign, the bronchial cutoff sign and the cavity sign in the three differentiated subgroups (χ^2=6.818~63.331, P<0.05). No significant differences were found in the air bronchogram sign and vacuole sign among the three differentiated subgroups (P>0.05). ***Conclusions*:** HRCT signs of lung adenocarcinoma are closely related to the pathological subtype and differentiation degree and have great value in helping predict tumor types and devise clinical treatment plans.

INTRODUCTION

The incidence and mortality rates of lung cancer remain the highest among all cancers worldwide [1, 2]. To date, squamous cell carcinoma (SCC) has been surpassed by lung adenocarcinoma as the most highly incident lung cancer [3], and adenocarcinoma is the most common histologic subtype of lung cancer in most countries, accounting for almost half of all lung cancers, which seriously threatens people's health and quality of life [4]. The lung cancer classification system launched by the World Health Organization (WHO) accepted the pathological classification method in 2015, which was cosponsored by the International Association for the Study of Lung Cancer, American Thoracic Society and European Respiratory Society in 2011 [5]. Lung adenocarcinomas are classified into atypical adenomatous hyperplasia (AAH), adenocarcinoma in situ (AIS), minimally invasive adenocarcinoma (MIA) and invasive adenocarcinoma (IAC) with adherent growth. Among them, AAH and AIS belong to the same pre-invasive lesion (PIL) category. Initial data studies using new classification methods in early resected adenocarcinoma have indicated significant prognostic differences between histological subtypes [6]. Therefore, the early identification of histopathological subtypes of lung adenocarcinoma has profound significance for the presurgical diagnosis and choice of clinical treatment plans.

At present, the diagnosis of pathological subtypes of lung adenocarcinoma mainly depends on invasive pathological examination, such as percutaneous puncture, endoscopic biopsy and surgery [7]. These methods can cause different degrees of damage to patients. Therefore, finding a safe, noninvasive and low-risk inspection method is an urgent clinical pro blem. At the present time, it is very important to distinguish the histological types of lung cancer. Both AIS and MIA have a 100% 5-year disease-free survival rate and a 100% 5-year overall survival rate after radical surgery [8]. However, there are many limitations in predicting different subtypes of adenocarcinoma from lung computed tomography (CT), such as the diverse radiomic descriptors and the difficulty of extracting effective radiomic descriptors from lung nodules. To overcome these challenges, a competing round-robin prediction

model was elucidated by Chen to predict the histological subtypes of lung adenocarcinoma. Based on 70 adenocarcinoma patients, the proposed model achieved an accuracy of 86.3% in predicting five histological subtypes of adenocarcinomas [9]. Then, 44 lung adenocarcinoma patients were studied by Cohen, finding that AIS and MIA were differentiated from IAC among subsolid lung nodules by CT [10]. In addition, the segmentation techniques of three-dimensional (3D) CT indicated that computer-assisted 3D measurement of nodules by CT had good reproducibility and help to differentiate among subtypes of lung adenocarcinoma [11]. Other studies on pathological subtypes of lung adenocarcinoma were proposed by Eriguchi e*t al.* [12-14].

Therefore, in this study, we tried to estimate the correlation between HRCT features and pathological subtype in lung adenocarcinoma. We also explore the relationships between such features and differentiation degree of IAC in lung adenocarcinoma. Furthermore, we'd like to find some valuable HRCT signatures which can help distinguish histological subtypes and differentiation of lung adenocarcinoma to predict their prognosis.

MATERIALS AND METHODS

Patient selection

A total of 394 hospitalized patients (226 males; 168 females; age range, 32-81 years; average age, 56.5±24.5 years) with subsequent histologic confirmation of lung adenocarcinoma were collected consecutively between October 2016 and September 2018. The inclusion criteria were histologically proven incident pulmonary lesions with complete chest HRCT imaging data. Exclusion criteria were received radiotherapy and chemotherapy. According to the pathological results, 394 patients were divided into the PIL group, MIA group and IAC group, and IAC was divided into three subgroups: high differentiation (HD), moderate differentiation (MD) and poor differentiation (PD). Demographic information of patients for different category was shown in table 1. This retrospective study was approved by the local Institutional Review Board and was conducted in accordance with the ethical standards of the Declaration of Helsinki. The Ethics code of this study was YX-P-2020-085-01 (date: 13/03/2020).

Table 1. Demographic characteristics of patients.

Pathology		Number of patient (%)		Gender		Age		
		No.	%	Female	Male	32-50	50-65	66-81
PIL		71	18.0	28	43	6	31	34
MIA		44	11.2	17	27	4	19	21
IAC		279	70.8	111	168	28	114	137
IAC	HD	95	24.1	41	54	10	41	44
	MD	66	16.8	25	41	6	26	34
	PD	118	29.9	45	73	12	47	59

HRCT imaging acquisition

The CT imaging was performed on a 64-detector row dual source CT scanner (SIEMENS SOMATOM Definition Flash, Germany) at the energy of 120 kVp in the mode of Care Dose 4D. The parameters of matrix were 512×512 voxel. The current of the tube was automatically adjusted. Reconstruction parameters include: Convolution kernel B80f, 1 mm slice thickness. Then, axial and additional sagittal and coronal images were obtained.

Analysis of imaging characteristics

Two chest radiologists with 10 and 8 years of experience in thoracic imaging who were blinded to the clinical and pathological data evaluated all images on both mediastinal (width, 350 HU; level, 50 HU) and lung (width, 1200 HU; level, -600 HU) windows. The characteristics of the lesion were as follows: 1) the lesion margin (smooth or irregular); 2) the lesion size (the average of the longest and shortest diameter of the maximum area of the tumor on the lung window image); 3) the lesion density; 4) the pleural traction sign; 5) the tumor vascular sign; 6) the spicule sign; 7) the lobulation sign; 8) the bronchial cutoff sign; 9) the air bronchogram sign; 10) the vacuole sign; and 11) the cavity sign. Evaluation and analysis of the images were performed. The radiologists sought to reach a consensus when there were dissimilar findings. The size of the lesions in the PIL group was 1.44±0.92 cm, that in the MIA group was 1.76±1.13 cm, and that in the IAC group was 3.52±2.41 cm. In this study, the lesion size was divided into three grades: ≤1.5 cm, 1.5-3 cm [15] and >3 cm [16], and the sizes were compared by the incidence of lesions in each group. The low density in noncalcified lesions demonstrated that they had more ground-glass components, while more solid components in lesions conferred a higher density. According to the density, the lesions were divided into three categories: pure ground-glass, mixed ground-glass and solid. The characteristics and the density of each group were compared, and then CT signs of each group were deduced.

Typical case images are presented in figures 1-5.

Statistical analysis

Statistical analysis was performed with IBM SPSS Statistics 22 Developer software packages. The size and density were analyzed by the Kruskal-Wallis test, and signs were analyzed by the chi-squared test. The corrected value and *P*-value were used when 1<T<5 and N >40; the *P*-value of Fisher's exact probability method was used when T<1 or N<40. In all tests, a *P*-value of <0.05 was considered statistically significant.

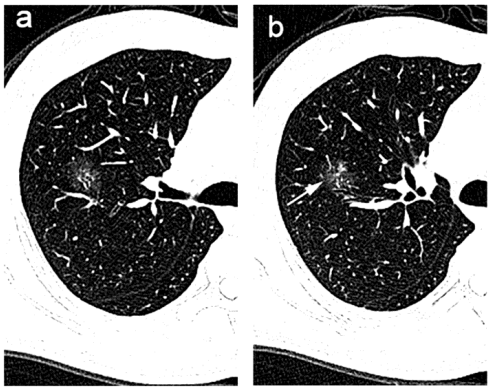

Figure 1. CT characteristics of a 46-year-old male patient. AAH of the segmental alveolar epithelium in the upper lobe of the right lung, with focal area reaching AIS. **(a)** CT plain scan showed the ground glass density of the lesion. The size was 29.6x24.1 mm, the margin was irregular and the air bronchogram sign was seen in the lesion. **(b)** Adjacent blood vessels shift and enter the interior of the lesion, which is known as the tumor vascular sign (arrow). AAH, atypical adenomatous hyperplasia; AIS, adenocarcinoma in situ.

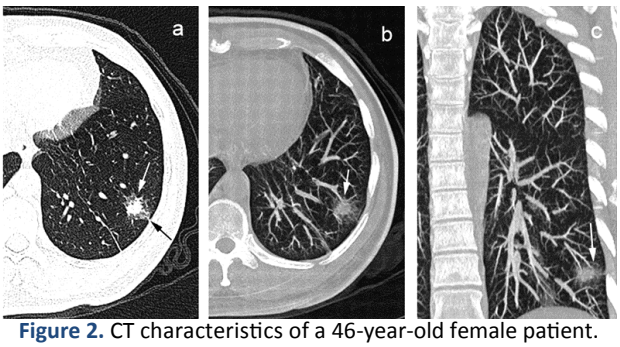

Figure 2. CT characteristics of a 46-year-old female patient. MIA of the left lower lobe of the lung. **(a)** CT plain scan showed mixed ground-glass density, dominated by solid density. The size of the lesion was about 25.9 × 20.9 mm. The margin was irregular and the lobulation sign (white arrow) and adjacent pleural traction (black arrow) could be observed. **(b)** The tumor vascular sign after MIP recombination. **(c)** The coronal position of the MIP recombination showed that blood vessels entered the lesion. MIA, minimally invasive adenocarcinoma; MIP, maximum intensity projection.

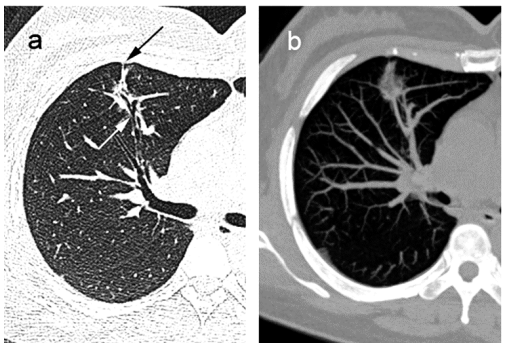

Figure 3. CT characteristics of a 52-year-old female patient with highly differentiated adenocarcinoma of the anterior segment of the right upper lobe. **(a)** CT plain scan showed that the lesion showed ground-glass density and was about 21.6×11.7 mm in size. The margin was irregular, the air bronchogram sign (white arrow) could be seen in the lesion, and the adjacent pleura was stretched and thickened (black arrow). **(b)** The MIP reconstruction showed multiple adjacent vessels entering the lesion (tumor vascular sign).

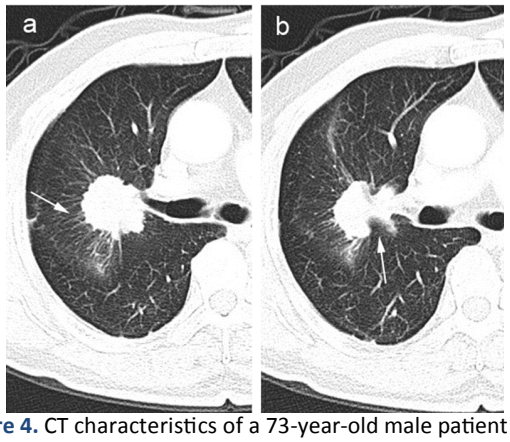

Figure 4. CT characteristics of a 73-year-old male patient with moderately differentiated adenocarcinoma of the right upper lobe. **(a)** CT plain scan showed that the lesion showed solid density and was about 42.3×37.1 mm in size. The margin was irregular, and the shallow lobulation sign, spicule sign (arrow) and pleural thickening could be seen in the lesion. **(b)** Deep lobulation can be seen around lesion margin (arrow).

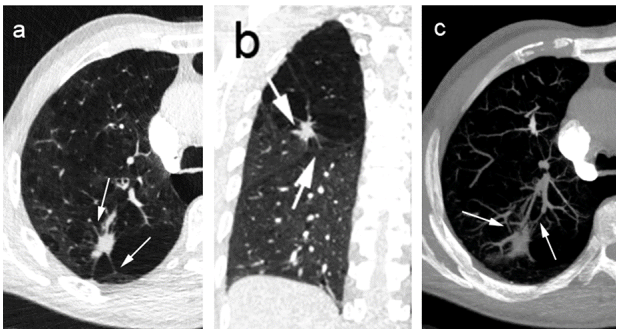

Figure 5. CT characteristics of a 62-year-old male patient with poorly differentiated adenocarcinoma of the right upper lobe. **(a)** CT plain scan showed that the lesion showed solid density and was about 19.6×10.3 mm in size. The spicule, lobulation and pleural traction signs (arrows) can be seen at the margin of the lesion, and emphysema changes can also be observed. **(b)** Sagittal position showed that the interlobar pleura was pulled and displaced, and the lobulation sign can be seen in the margin of the lesion (arrow). **(c)** The tumor vascular sign (arrow) was observed after the MIP recombination (arrow).

RESULTS

Histopathological subtypes and HRCT signs

The HRCT features of 394 patients in different groups of histopathological subtypes were extracted and analyzed. The relationship between different pathological subtypes and these signs are expressed in table 2.

There was no significant difference in HRCT signs between PILs and MIA (P>0.05). In the IAC group, the incidence of lesions that were ≤1.5 cm in diameter and categorized as pure ground glass was the lowest (P<0.05). Meanwhile, the IAC group had the highest incidence of lesions that were >3 cm in diameter and solid (P<0.05). However, lesions with sizes between 1.5 and 3 cm in the MIA group had a higher incidence than those in the IAC group (P<0.05). The incidences of the pleural traction sign, spicule sign, lobulation sign, tumor vascular sign, bronchial cutoff sign, air

bronchogram sign and cavity sign in the IAC group were significantly higher than those in the PIL group and MIA group (P<0.05). The incidences of all these signs (except the cavity sign) in IAC were higher than those in the other two groups (P<0.05); the incidence of the cavity sign in IAC was higher than that in PILs (P<0.01) but not higher than that in MIA (P>0.05). These groups were not significantly associated with the incidence of margin irregularity and the vacuole sign (P=0.338 and P=0.279, respectively).

Table 2. Correlation of HRCT signs with histopathological subtypes of lung adenocarcinoma.

A: Relationship of size and density with pathology.

Pathology	Size ≤ 1.5 cm	Size 1.5~3 cm	Size > 3 cm	Pure ground-glass	Mixed ground-glass	Solid
PIL	28*	43	0*	57*	14	0*
MIA	11#	33#	0#	31#	12	1#
IAC	8*,#	137#	134*,#	11*,#	49	219*,#
H-value	120.854			247.077		
P-value	0.000			0.000		

B: Relationship of margin irregularity, plural traction sign and spicule sign with pathology.

Pathology	Margin irregularity +	Margin irregularity -	Pleural traction sign+	Pleural traction sign -	Spicule sign +	Spicule sign -
PIL	50	21	22*	49	5*	66
MIA	32	12	17#	27	4#	40
IAC	218	61	186*,#	93	163*,#	116
χ^2-value	2.172		36.315		84.801	
P-value	0.338		0.000		0.000	

C: Relationship of the lobulation sign, tumor vascular sign and bronchial cut-off sign with pathology

Pathology	Lobulation sign +	Lobulation sign -	Tumor vascular sign+	Tumor vascular sign -	Bronchial cutoff sign +	Bronchial cutoff sign -
PIL	10*	61	3*	68	0*	71
MIA	5#	39	3#	41	1#	43
IAC	146*,#	133	107*,#	172	72*,#	207
χ^2-value	52.095		43.797		43.790	
P-value	0.000		0.000		0.000	

D: Relationship of the air bronchogram sign, vacuole sign and cavity sign with pathology

Pathology	Air bronchogram sign +	Air bronchogram sign -	Vacuole sign+	Vacuole sign -	Cavity sign +	Cavity sign -
PIL	10*	61	3	68	0*	71
MIA	7#	37	1	43	0	44
IAC	122*,#	157	23	256	31*	248
χ^2-value	29.920		2.477		16.308	
P-value	0.000		0.279		0.001	

Note: Table A. Kruskal-Wallis test; Table B-D. Chi-square test. PIL: Preinvasive Lesions, MIA: Minimally Invasive Adenocarcinoma, IAC: Invasive Adenocarcinoma. *comparison of PIL and IAC, P<0.05; #comparison of MIA and IAC， P<0.05.

Differentiation subtypes of IAC and HRCT signs

The relationship between different differentiation subtypes and HRCT signs are expressed in table 3. The incidence of lesions >3 cm in diameter was lowest in the subtype of high differentiation, while the incidence of lesions between 1.5 cm and 3 cm was significantly higher in the highly differentiated subgroup than in the other two subgroups (*P*<0.05). The incidence of solid lesions was highest in the poorly differentiated subgroup, while the occurrence rate of mixed ground-glass lesions in the poorly differentiated subgroup was lower than that of the other two subgroups (*P*<0.05). There were significant differences in the incidences of margin irregularity among the three differentiated subgroups (*P*=0.033). The incidences of the pleural traction sign, tumor vascular sign and cavity sign in the poorly differentiated subgroup were significantly higher than those in the highly and moderately differentiated subgroups (*P*<0.05), but there was no significant difference between the moderately and highly differentiated subgroups (*P*>0.05). The incidence of the spicule sign and bronchial cutoff sign in the poorly differentiated subgroup was higher than that in the highly differentiated subgroup, while the occurrence rate of the lobulation sign in the highly differentiated subgroup was the lowest among the subgroups (*P*<0.05). These subgroups were not significantly associated with the incidence of the air bronchogram sign and vacuole sign (*P*>0.05).

Table 3. Correlation of size and density with different differentiation degrees of IAC.

A: Relationship of size and density with different differentiation degrees.

Pathology	Size≤1.5m	Size 1.5~3 cm	Size>3 cm	Pure ground-glass	Mixed ground-glass	Solid
HD	7*	72©,*	16©,*	10*	28*	57*
MD	1	29©	36©	1	14#	51#
PD	0*	36*	82*	0*	7*,#	111*,#
H-value	63.331			37.719		
P-value	0.000			0.000		

B: Relationship of margin irregularity, the plural traction sign and the spicule sign with different differentiation degrees.

Pathology	Margin irregularity +	Margin irregularity -	Plural traction sign +	Plural traction sign -	Spicule sign +	Spicule sign -
HD	68	27	54*	41	43*	52
MD	49	17	37#	29	36	30
PD	101	17	95*, #	23	84*	34
χ^2-value	6.818		17.641		15.095	
P-value	0.033		0.000		0.001	

C: Relationship of the lobulation sign, tumor vascular sign and bronchial cut-off sign with different differentiation degrees.

Pathology	Lobulation sign +	Lobulation sign -	Tumor vascular sign +	Tumor vascular sign -	Bronchial cutoff sign +	Bronchial cutoff sign -
HD	35 ◎, *	60	22*	73	11*	84
MD	39◎	27	20#	46	15	51
PD	72*	46	65*, #	53	46*	72
χ^2-value	13.914		25.058		21.071	
P-value	0.001		0.000		0.000	

D: Relationship of the air bronchogram sign, vacuole sign and cavity sign with different differentiation degrees.

Pathology	Air bronchogram sign +	Air bronchogram sign -	Vacuole sign +	Vacuole sign -	Cavity sign +	Cavity sign -
HD	49	46	8	87	1*	94
MD	23	43	4	62	4#	62
PD	50	68	11	107	26*, #	92
χ^2-value	4.583		0.601		25.690	
P-value	0.101		0.740		0.000	

Note: Table A. Kruskal-Wall test; Table B-D. Chi-square test. HD: High Differentiation, MD: Moderate Differentiation, PD: Poor Differentiation. ◎, comparison of HD and MD, P<0.05; #, comparison of HD and PD, P<0.05; *, comparison of MD and PD, P<0.05.

DISCUSSION

In our study, the IAC group had the highest incidence of lesions >3 cm in diameter and solid, while the lowest incidence of lesions ≤1.5 cm in diameter and pure ground-glass. There was no significant difference in the sizes of PIL and MIA tumors (*P*>0.05). Recent research has reported that the degree of infiltration for lung adenocarcinoma was positively correlated with the size and density of the lesion, and the average axial diameter of IAC is larger than that of non-IAC lesions [17, 18], which is consistent with the results of our study. Pure ground-glass density lesions accounted for 80.3%, 70.5% and 3.9% of PILs, MIA and IAC in our study. In the results of Heidinger *et al.* [19], the incidence of pure ground-glass density lesions in PILs, MIA and IAC were 44%, 40% and 16%. The differences may be due to the latter study only collected pure ground-glass density lesions.

In this study, the incidence of lesions with sizes of 1.5~3 cm were significantly higher in the highly differentiated subgroup than those in the other two groups (*P*<0.05). Lesions with sizes greater than 3 cm accounted for 69.5% in the poorly differentiated subgroup, which was significantly higher than that in the other two groups (*P*<0.05). The incidence of pure ground-glass lesions in the highly differentiated subgroup was significantly higher than that in the poorly differentiated subgroup. Solid lesions accounted for the largest proportion of cases (94.1%) in the poorly differentiated subgroup (*P*<0.05). The density and size of the lesions gradually increased with the degree of differentiation of IAC, which is consistent with the results of previous studies [20, 21].

The pleural traction sign, lobulation sign, spicule sign, tumor vascular sign, bronchial cutoff sign cavity sign and air bronchogram sign had higher proportions in the IAC group than in the PIL and MIA groups (*P*<0.05). Oda *et al.* [22] reported that the occurrence rate of the spicule sign of IAC was higher than that of PIL, which is consistent with our study. The formation of the lobulation sign is mainly related to the different growth rates of lesions in different directions and growth restriction around the tumor [23]. The lobulation sign, especially the deep lobulation sign, often indicates malignant lesions [24]. According to the study of Lee *et al.* [25], the lobulation sign is of great significance in the differential diagnosis between IAC and non-IAC. The findings of our study suggest that the incidence of the lobulation sign in the IAC group was significantly higher than that in the PIL and MIA groups, which was consistent with the abovementioned view.

The incidences of the spicule sign and bronchial cutoff sign in the poorly differentiated subgroup were higher than those in the highly differentiated subgroup, while the lobulation sign had the lowest incidence in the highly differentiated subgroups (P<0.05), which was consistent with the findings of a previous study [26].The results of previous studies [27-29] showed that the incidences of the lobulation, spicule and pleural traction signs of lung adenocarcinoma differed between highly and poorly differentiated adenocarcinoma. In our study, the pleural traction sign, tumor vascular sign and cavity sign in the poorly differentiated subgroup were significantly higher than those in the other two subgroups (P< 0.05). These differences could be related to the different grouping methods of these

studies.

Xiang *et al.* [30] reported that the air bronchogram sign is meaningful for predicting the infiltration degree of lung adenocarcinoma. Another study showed that the air bronchogram sign has vital significance in the differential diagnosis between IAC and non-IAC [31]. Zheng *et al.* [32] suggested that the bronchi present as a cut-off due to strangulation and obliteration when the tumor invades the bronchial wall. There was no significant difference in the air bronchogram sign but there was a significant difference in the bronchial cutoff sign in the three differentiated subgroups of this investigation. Therefore, the interruption of inflatable bronchial segments in the lesions mostly suggests the presence of a malignant tumor.

The vacuole sign is a gassy, lucent shadow with a diameter of <5 mm, which refers to local bronchiectasis and alveolar enlargement caused by residual pneumonic tissue or local obstruction in the tumor. Some researchers have suggested that the vacuole sign can indicate benign or malignant lesions [33] but has no significance for the degree of infiltration of malignant nodules [34, 35]. All the cases in this study were proven to be lung adenocarcinoma by pathology, and there was no difference in the incidence of the vacuole sign in PILs, MIA and IAC, nor in the three subgroups of IAC, which is consistent with the above results.

There were several limitations to our study. First, this paper is a retrospective study, and the vascular and solid components were difficult to distinguish in some cross-sections of the lesions. Second, all the data were measured manually. Therefore, errors in the results are inevitable. Finally, due to the limited sample size, the results may be biased. Hence, the accuracy of the conclusion needs to be further verified to overcome these limitations in the future.

CONCLUSION

It can be concluded that lung adenocarcinoma and its histopathological subtype and degree of differentiation are related to its imaging features. The histological subtype and differentiation of lung adenocarcinoma can be predicted based on the imaging features of the lesions, which is important for early diagnosis of partially curable subtypes of lung adenocarcinoma, guiding surgical selection and postoperative outcome assessment.

ACKNOWLEDGEMENTS

None.

***Funding*:** The project was supported by the science and technology development fund of Nanjing medical University (No. 2016NJMUZD085).

***Ethical considerations*:** This retrospective study was approved by the research Ethics Committee of Huai'an First People's Hospital with the number YX-P -2020-085-01 at 13th March 2020.

***Conflicts of interest*:** The authors declare no conflicts of interest.

***Author contributions*:** (I) Conception and design: LL Guo; (II) Provision of study materials or patients: G Bo; (III) Collection and assembly of data: LZ Duan and WL Shan; (IV) Data analysis and interpretation: LZ Duan; (V) Manuscript writing: LL Guo and LZ Duan; (VI) Final approval of manuscript: All authors.

REFERENCES

1. Boyle P and Levin B (2008) World cancer report 2008[M]. *IARC Press, International agency for research on cancer, 2008*.
2. Torre LA, Bray F, Siegel RL, *et al.* (2015) Global cancer statistics 2012. *CA Cancer J Clin, **65**(2): 87-108*.
3. Blom JW, Osanto S, Rosendaal FR (2004) The risk of a venous thrombotic event in lung cancer patients: higher risk for adenocarcinoma than squamous cell carcinoma. *J Thromb Haemost, **2**(10): 1760-5*.
4. Coroller TP, Grossmann P, Hou Y, *et al.* (2015) CT-based radiomic signature predicts distant metastasis in lung adenocarcinoma. *Radiother Oncol, **114**(3): 345-50*.
5. Travis WD, Brambilla E, Noguchi M, *et al.* (2011) International association for the study of lung cancer/American thoracic society/European respiratory Society: international multidisciplinary classification of lung adenocarcinoma: executive summary. *Journal of Thoracic Oncology, **6**(2): 244-85*.
6. Fujimoto Y, Togo S, Tulafu M, *et al.* (2015) Variation in the expression levels of predictive chemotherapy biomarkers in histological subtypes of lung adenocarcinoma: an immunohistochemical study of tissue samples. *Int J Clin Exp Pathol, **8**(9): 10523-33*.
7. Shimamura Y, Sasaki S, Shimohira M, *et al.* (2018) New technique of percutaneous CT fluoroscopy-guided marking before video-assisted thoracoscopic surgery for small lung lesions: feasibility of using a 25-gauge needle without local anaesthesia. *The British Journal of Radiology, **91**: 20170692*.
8. Gu J, Lu C, Guo J, *et al.* (2013) Prognostic significance of the IASLC/ATS/ERS classification in Chinese patients-a single institution retrospective study of 292 lung adenocarcinoma. *J Surg Oncol, **107**(5): 474-80*.
9. Chen L, Yang S, Wang HJ, *et al.* (2018) A competing round-robin prediction model for histologic subtype prediction of lung adenocarcinomas based on thoracic computed tomography. *Int Soci for Optics and Photonics, **10578**: 105782M*.
10. Cohen J G, Reymond E, Medici M, *et al.* (2018) CT-texture analysis of subsolid nodules for differentiating invasive from in-situ and minimally invasive lung adenocarcinoma subtypes. *Diagn Interv Imaging, **99**(5): 291-9*.
11. Ko JP, James S, Opeyemi I, *et al.* (2016) Lung adenocarcinoma: Correlation of quantitative CT findings with pathologic findings. *Radiology, **280**(3): 931-9*.
12. Eriguchi D, Shimada Y, Imai K, *et al.* (2018) Predictive accuracy of lepidic growth subtypes in early-stage adenocarcinoma of the lung by quantitative CT histogram and FDG-PET. *Lung Cancer, **125**: 14-21*.
13. Linning E, Lin L, Li L, *et al.* (2019) Radiomics for classification of lung cancer histological subtypes based on nonenhanced computed tomography. *Acad Radiol, **26**(9): 1245-52*.
14. Xiaoli XU, Sui X, Zhong W, *et al.* (2018) Diagnostic value of quantitative dual-source CT dual-energy iodine maps combined with morphological CT features in assessing histological subtypes of lung cancer. *Chinese Journal of Radiology, **52**(11): 823-8*.
15. Winer-Muram HT (2006) The solitary pulmonary nodule. *Radiology, **239**(1): 34-49*.
16. Jeong YJ, Yi CA, Lee KS (2008) Solitary pulmonary nodules: detection, characterization, and guidance for further diagnostic workup and treatment. *AJR Am J Roentgenol, **188**(1): 183-95*.
17. Moon Y, Sung SW, Lee KY, *et al.* (2016) Pure ground-glass opacity on chest computed tomography: predictive factors for invasive adenocarcinoma. *Journal of Thoracic Disease, **8**(7): 1561*.

18. Heidinger BH, Anderson KR, Nemec U, *et al.* (2017) Lung adenocarcinoma manifesting as pure ground-glass nodules: correlating CT size, volume, density, and roundness with histopathologic invasion and size. *Journal of Thoracic Oncology,* ***12****(8): 1288-98*.
19. Eguchi T, Yoshizawa A, Kawakami S, *et al.* (2014) Tumor size and computed tomography attenuation of pulmonary pure ground-glass nodules are useful for predicting pathological invasiveness. *PLoS,* ***9****(5)*.
20. Henschke CI, Yankelevitz DF, Naidich DP, *et al.* (2004) CT screening for lung cancer: suspiciousness of nodules according to size on baseline scans. *Radiology,* ***231****(1): 164-8*.
21. Cho J, Ko SJ, Kim SJ, *et al.* (2014) Surgical resection of nodular ground-glass opacities without percutaneous needle aspiration or biopsy. *BMC Cancer,* ***14****(1): 838*.
22. Oda S, Awai K, Liu D, *et al.* (2008) Ground-glass opacities on thin-section helical CT: differentiation between bronchioloalveolar carcinoma and atypical adenomatous hyperplasia. *American J Roentgenology,* ***190****(5): 1363-8*.
23. Gao F, Li M, Ge X, *et al.* (2013) Multi-detector spiral CT study of the relationships between pulmonary ground-glass nodules and blood vessels. *European Radiology,* ***23****(12): 3271-7*.
24. She Y, Zhao L, Dai C, *et al.* (2017) Preoperative nomogram for identifying invasive pulmonary adenocarcinoma in patients with pure ground-glass nodule: A multi-institutional study. *Oncotarget,* ***8****(10): 17229*.
25. Yoshino I, Nakanishi R, Kodate M, *et al.* (2000) Pleural retraction and intra-tumoral air-bronchogram as prognostic factors for stage I pulmonary adenocarcinoma following complete resection. *International Surgery,* ***85****(2): 105-12*.
26. Meng Y, Liu CL, Cai Q, *et al.* (2019) Contrast analysis of the relationship between the HRCT sign and new pathologic classification in small ground glass nodule-like lung adenocarcinoma. *Radiol Med,* ***124****(1): 8-13*.
27. Zhang Y, Shen Y, Qiang JW, *et al.* (2016) HRCT features distinguishing pre-invasive from invasive pulmonary adenocarcinomas appearing as ground-glass nodules. *Eur Radiol,* ***26****(9): 2921-8*.
28. Wang X, Duan H, Li X, *et al.* (2020) A prognostic analysis method for non-small cell lung cancer based on the computed tomography radiomics. *Phys Med Biol,* ***65****(4): 045006*.
29. Wang X, Lv L, Zheng Q, *et al.* (2018) Differential diagnostic value of 64-slice spiral computed tomography in solitary pulmonary nodule. *Exp Ther Med,* ***15****(6): 4703-8*.
30. Wahidi MM, Govert JA, Goudar RK, *et al.* (2007) Evidence for the treatment of patients with pulmonary nodules: when is it lung cancer?: ACCP evidence-based clinical practice guidelines (2nd edition). *Chest,* ***132****(3): 94S-107S*.
31. Lee SM, Park CM, Goo JM, *et al.* (2013) Invasive pulmonary adenocarcinomas versus preinvasive lesions appearing as ground-glass nodules: differentiation by using CT features. *Radiology,* ***268*** *(1): 265-73*.
32. Xiang W, Xing Y, Jiang S, *et al.* (2014) Morphological factors differentiating between early lung adenocarcinomas appearing as pure ground-glass nodules measuring≤ 10 mm on thin-section computed tomography. Cancer Imaging, **14**(1): 33.
33. Si MJ, Tao XF, Du GY, *et al.* (2016) Thin-section computed tomography–histopathologic comparisons of pulmonary focal interstitial fibrosis, atypical adenomatous hyperplasia, adenocarcinoma in situ, and minimally invasive adenocarcinoma with pure ground-glass opacity. *European Journal of Radiology,* ***85****(10): 1708-15*.
34. Zheng B, Zhou X, Chen J, *et al.* (2015) A modified model for preoperatively predicting malignancy of solitary pulmonary nodules: an Asia cohort study. *Ann Thorac Surg,* ***100****(1): 288-94*.
35. Yang ZG, Sone S, Takashima S, *et al.* (2001) High-resolution CT analysis of small peripheral lung adenocarcinomas revealed on screening helical CT. *AJR Am J Roentgenol,* ***176****(6): 1399-407*.
36. Liang J, Xu XQ, Xu H, *et al.* (2015) Using the CT features to differentiate invasive pulmonary adenocarcinoma from pre-invasive lesion appearing as pure or mixed ground-glass nodules. *Br J Radiol,* ***88****(1053): 20140811*.
37. Liu LH, Liu M, Wei R, *et al.* (2015) CT findings of persistent pure ground glass opacity: can we predict the invasiveness. *Asian Pac J Cancer Prev,* ***16****(5): 1925-8*.